ACS central science

Research Article

Cite This: ACS Cent. Sci. 2018, 4, 112−119

When NiO@Ni Meets WS_2 Nanosheet Array: A Highly Efficient and Ultrastable Electrocatalyst for Overall Water Splitting

Dewen Wang,[†,‡] Qun Li,[†,‡] Ce Han,[†] Zhicai Xing,*[,†] and Xiurong Yang*[,†]

[†]State Key Laboratory of Electroanalytical Chemistry, Changchun Institute of Applied Chemistry, Chinese Academy of Sciences, Changchun 130022, Jilin, China

[‡]University of Science and Technology of China, Hefei 230026, China

Supporting Information

ABSTRACT: The development of low-cost, high-efficiency, and stable bifunctional electrocatalysts toward the hydrogen evolution reaction (HER) and oxygen evolution reaction (OER) is of paramount importance for large-scale water splitting. Here, we develop a new strategy for the first design and synthesis of a NiO@Ni decorated WS_2 nanosheet array on carbon cloth (NiO@Ni/WS_2/CC) composite. This composite serves as a unique three-dimensional (3D) synergistic electrocatalyst that not only combines the intrinsic properties of individual NiO@Ni and WS_2, but also exhibits significantly improved HER and OER activities when compared to that of pure NiO@Ni and WS_2. This electrocatalyst possesses Pt-like activity for HER and exhibits better OER performance than that for commercial RuO_2, as well as demonstrating superior long-term durability in alkaline media. Furthermore, it enables an alkaline electrolyzer with a current density of 10 mA cm^{-2} at a cell voltage as 1.42 V, which is the lowest one among all reported values to date. The excellent performance is mainly attributed to the unique 3D configuration and multicomponent synergies among NiO, Ni, and WS_2. Our findings provide a new idea to design advanced bifunctional catalysts for water splitting.

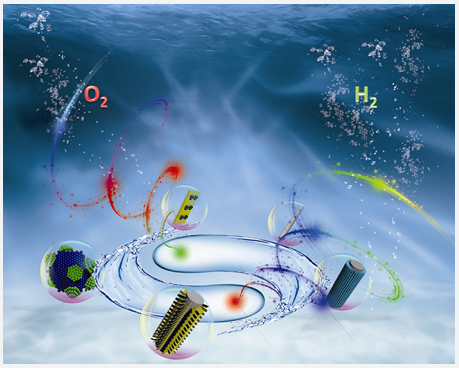

INTRODUCTION

Developing renewable clean energy is important for addressing the growing energy consumption and environmental pollution.[1] Hydrogen, as a clean fuel with high gravimetric energy density, has aroused wide attention.[2−4] Water electrolysis, including the hydrogen evolution reaction (HER) and oxygen evolution reaction (OER), is a sustainable way to produce hydrogen of high purity on a large-scale and store energy from renewable sources.[5−8] Owing to the scarcity and high price, the state-of-the-art catalysts of the HER (Pt-based noble metals)[9] and OER (Ru- and Ir-based oxides)[10,11] have not been widely used. Currently, searching for efficient and inexpensive alternative electrocatalysts has been actively pursued.[12] Although many meaningful progresses have been made,[13] most of them ignore the development of bifunctional electrocatalysts for promoting both HER and OER activity.[14] Such bifunctional electrocatalysts have practical application value in that neither different HER or OER catalysts nor additional device integration is needed.[15] The HER and OER catalysts controllably integrated into a single nanostructure is a potential way to design synergetic bifunctional electrocatalysts for both HER and OER in the past few years.[16]

Recently, layered transition metal dichalcogenides such as MoS_2 and WS_2 have been demonstrated to catalyze the HER.[17−19] Their graphite-like structures consist of stacked, weakly interacting layers held together by van der Waals interactions to form hexagonal structures.[20,21] Although MoS_2 is more well-known than WS_2 as an HER catalyst, the WS_2 also exhibits promising HER activities. However, many inherent factors of WS_2 have enormously limited its further applications for electrocatalysis: (1) The low density and reactivity of active sites. (2) Poor electrical transfer and inefficient electrical contact between the substrate and catalyst.[22] (3) The limited corrosion stability—all of the WS_2 applied to HER is in acidic media. (4) The electrocatalytic behavior of WS_2 for OER has been paid less attention. Meanwhile, because of the good electrical conductivity of metal Ni and the synergistic coupling of NiO and Ni, a few NiO@Ni based composites were used as electrocatalysts toward HER or OER.[23−25] As far as we know, the synergetic effects of an NiO@Ni-WS_2 system for overall water splitting has not been reported before, so we believe the combination of NiO@Ni and WS_2 array should be a desirable way to synthesize an active electrocatalysts toward water splitting.[26]

Herein, we synthesize a novel electrocatalyst of NiO@Ni decorated WS_2 nanosheet array on carbon cloth (NiO@Ni/WS_2/CC) for overall water splitting. WS_2 nanosheet array (WS_2/CC) was innovatively achieved through the sulfuration of the hydrothermally obtained WO_3/CC,[27] and then NiO@Ni was coated on WS_2/CC via electrodeposition of Ni and subsequently thermal oxidation in the oven (see Figure 1 and Methods, see Supporting Information for details). The unique NiO@Ni/WS_2/CC hybrid exhibits significant enhancement in

Received: October 19, 2017
Published: December 7, 2017

DOI: 10.1021/acscentsci.7b00502
ACS Cent. Sci. 2018, 4, 112−119

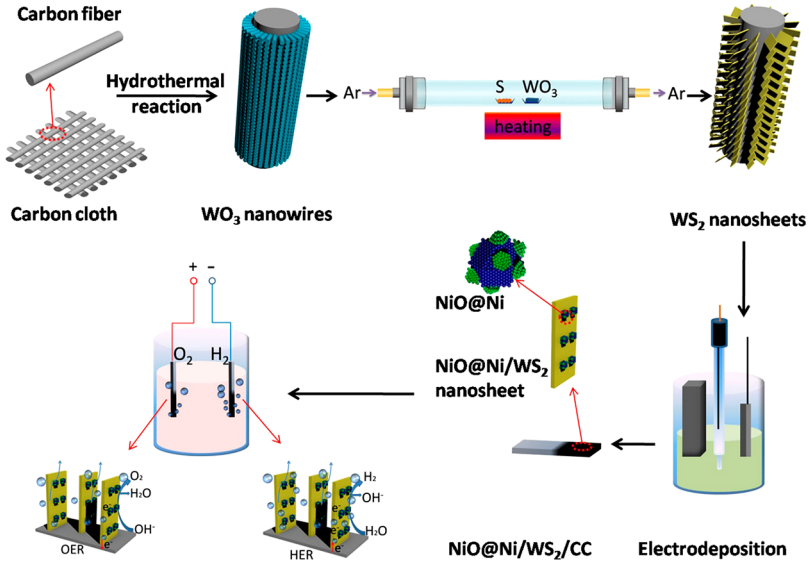

Figure 1. Schematic illustration of the preparation procedure for the NiO@Ni/WS_2/CC.

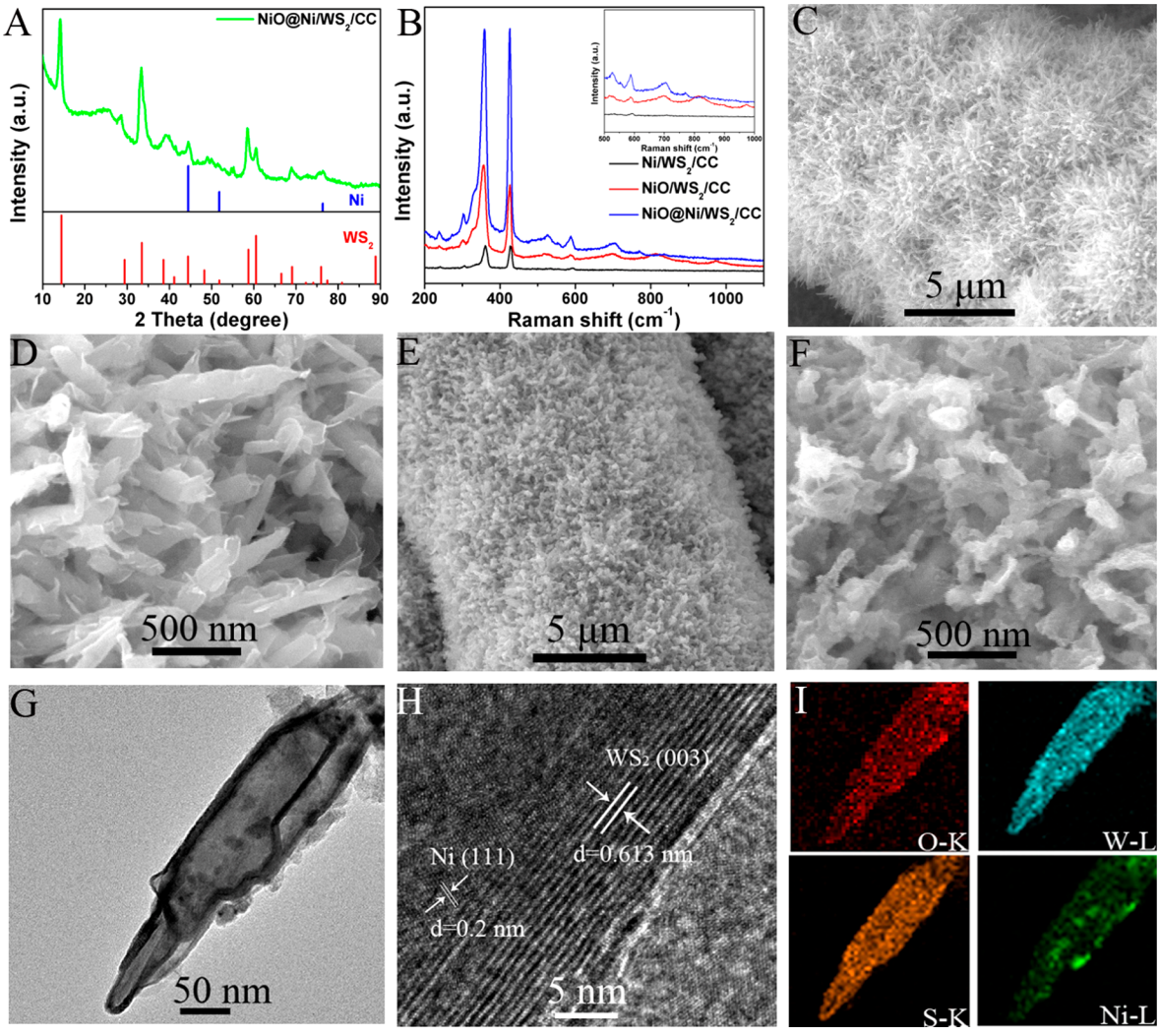

Figure 2. (A) XRD pattern of NiO@Ni/WS_2/CC. (B) Raman spectra of Ni/WS_2/CC, NiO/WS_2/CC, and NiO@Ni/WS_2/CC. SEM images of (C, D) WS_2/CC and (E, F) NiO@Ni/WS_2/CC. (G) TEM image of one single NiO@Ni/WS_2 nanosheet. (H) HRTEM image taken from the NiO@Ni/WS_2 nanosheet. (I) EDX elemental mapping images of an individual NiO@Ni/WS_2 nanosheet.

DOI: 10.1021/acscentsci.7b00502
ACS Cent. Sci. 2018, 4, 112−119

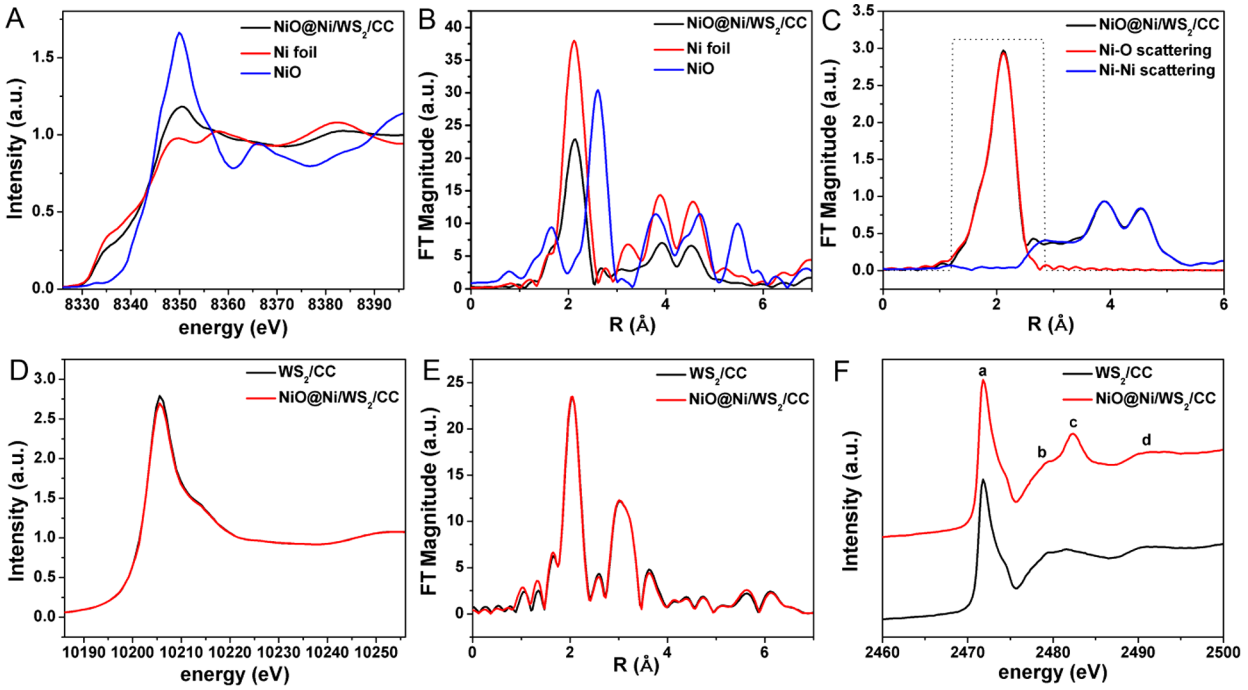

Figure 3. (A) The XANES spectra of Ni K-edge. (B) The Fourier transforms of k3-weighted Ni K-edge EXAFS spectra for NiO@Ni/WS_2/CC, Ni foil and NiO. (C) Observed (black line) and calculated (red and blue line) Fourier transforms of k3-weighted Ni K-edge EXAFS spectra for NiO@Ni/WS_2/CC. (D) The XANES spectra of W K-edge. (E) Fourier transforms of k3-weighted W K-edge EXAFS spectra for WS_2/CC and NiO@Ni/WS_2/CC. (F) The XANES spectra of Ni K-edge for WS_2/CC and NiO@Ni/WS_2/CC.

both HER and OER performance and superior durability. As an HER cathode, it achieves a current density of 10 mA cm^{-2} at an overpotential of 40 mV, which is comparable to that of commercial Pt/C and superior to many other previously reported catalysts. When used as an OER anode, it only needs an overpotential of 347 mV to drive 50 mA cm^{-2}, which is much better than that of commercial RuO_2. Notably, NiO@Ni/WS_2/CC affords the current density of 10 mA cm^{-2} at a voltage of only 1.42 V for alkaline electrolyzer, which is the best performance of two electrodes setup at present as far as we know. The possible multicomponent synergies among NiO, Ni, and WS_2 were systematically analyzed, rendering them simultaneously highly active for the HER and OER.

RESULTS AND DISCUSSION

Figure 2A shows the XRD pattern of NiO@Ni/WS_2/CC; there are six diffraction peaks at 14.4, 33.5, 38.6, 44.4, 48.3, and 60.5° which index to the (003), (101), (104), (009), (107), and (1010) planes of WS_2, respectively (JCPDS 35-0651).[28] The three additional diffraction peaks at 44.5, 51.8, and 76.4° corresponded to the (111), (200), and (220) of metallic Ni, respectively (JCPDS 65-2865).[29] The NiO peaks are not obvious because the NiO is too thin to be detected.[24] Raman spectra show two characteristic peaks around 356 and 418 cm^{-1}, which are originated from WS_2;[30] meanwhile, five peaks at 528, 590, 702, 818, and 974 cm^{-1} are attributed to NiO, indicating the existence of NiO in NiO@Ni/WS_2/CC (Figure 2B).[31] The scanning electron microscopy (SEM) images (Figure S1) show that WO_3 nanowires are homogeneously coated on CC. Figure 2C,D demonstrates that the WO_3 nanowires are all transformed into nanosheets after sulfuration. The thickness and roughness of nanosheets are increasing after coating NiO@Ni on WS_2/CC (Figure 2E,F). The low magnification transmission electron microscopy (TEM) image for one single NiO@Ni/WS_2 nanosheet was displayed in Figure 2G with a length and width of 370 and 80 nm, respectively. The high resolution transmission electron microscopy (HRTEM) image of NiO@Ni/WS_2 (Figure 2H) shows two distinguished phases: layered WS_2 and crystallized Ni. The interlayer spacing of 0.613 nm between the stripes of WS_2 can be observed,[32] and the typical interfringe distance of 0.20 nm for Ni is identified.[33] Several bright rings in the corresponding selective area electron diffraction (SAED) pattern are indexed to the planes of Ni and WS_2 (Figure S2). The scanning TEM (STEM) image (Figure S3) and the energy dispersive X-ray spectrum (EDX) elemental mapping images of NiO@Ni/WS_2 (Figure 2I) indicate a homogeneous dispersion of O, W, S, and Ni throughout the nanosheet. N_2 physisorption measurement is performed to verify the Brunauer−Emmett−Teller (BET) surface area of as-prepared catalyst (Figure S4). The BET surface area of NiO@Ni/WS_2/CC is measured to be as large as 335 m^2 g^{-1}.

The surface elemental composition and valence state of the composite are detected by X-ray photoelectron spectroscopy (XPS). The peaks of Ni $2p_{3/2}$ and Ni $2p_{1/2}$ at 855.5 and 873.2 eV are attributed to characteristic features of Ni^{2+}, and a weak peak at 852.7 eV corresponds to metallic Ni (Figure S5A), suggesting the existence of Ni^{2+} and metallic Ni on the surface.[34] The other two peaks at higher binding energies around 860.9 and 879.7 eV are shakeup type peaks of Ni. The O 1s spectrum displays four peaks (Figure S5B): the one at 529.5 eV is associated with a Ni−O bonds, and the other three peaks of 531.2, 531.9, and 532.9 eV are usually attributed to the defects and surface substances.[35] The W^{4+} reflect in the peaks of 32.8 (W $4f_{7/2}$) and 34.9 eV (W $4f_{5/2}$) (Figure S5C). Another weak peak located at 38.2 eV can be attributed to a W valence higher than +4. Besides the two well-known peaks for S $2p_{3/2}$ and S $2p_{1/2}$ at 162.2 and 163.4 eV (Figure S5D),[36] respectively, a new peak at 168.3 eV should be assigned to S^{6+}, implying an

DOI: 10.1021/acscentsci.7b00502
ACS Cent. Sci. 2018, 4, 112−119

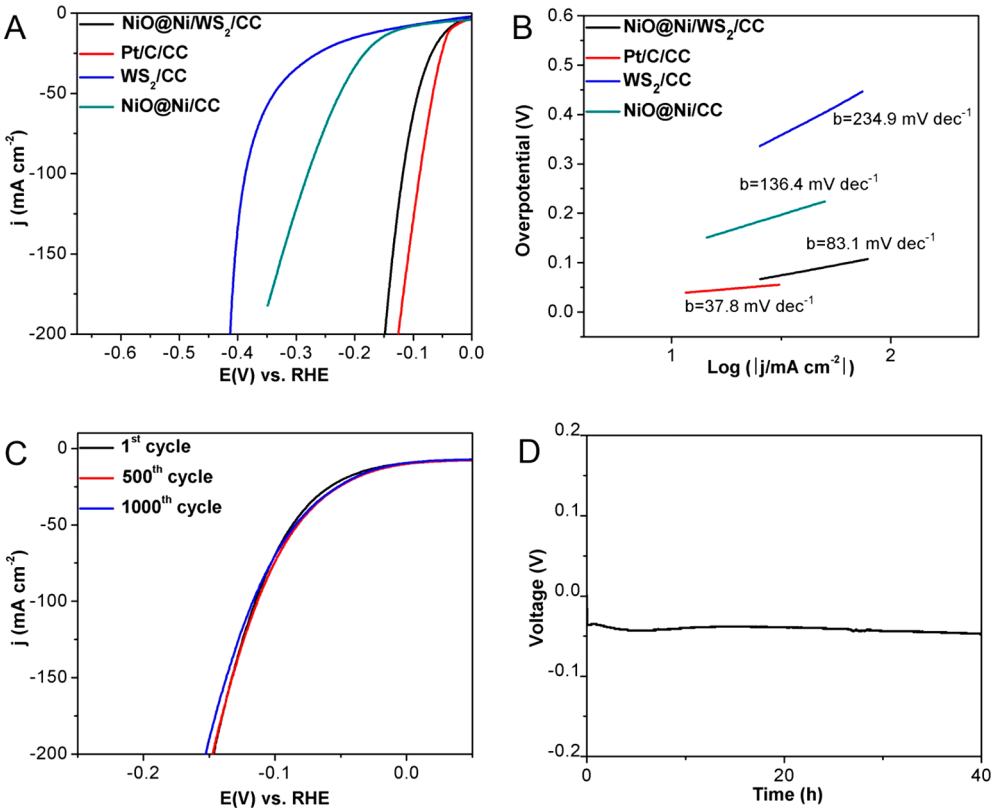

Figure 4. (A) The LSV curves for NiO@Ni/WS_2/CC, WS_2/CC, Pt/C/CC, and NiO@Ni/CC with a scan rate of 5 mV s^{-1} for HER. (B) The corresponding Tafel plots. (C) LSV curves for NiO@Ni/WS_2/CC initially, after 500 and 1000 CV cycles. (D) Potentiostatic electrolysis of NiO@Ni/WS_2/CC for 40 h with a scan rate of 5 mV s^{-1}.

inevitable surface oxidation of S species. It is worth noting that the Ni 2p binding energies of 852.7, 855.5, and 873.2 eV for NiO@Ni/WS_2/CC are positively shifted from those for Ni metal (852.5, 854.8, and 872.5 eV), while the S 2p binding energies of 162.2 and 163.4 eV are negatively shifted from element S (162.8 and 163.95 eV) for WS_2/CC (Figure S6), which indicates the electron transfer from Ni to S and a strong interaction between WS_2 and NiO@Ni.[37] The binding energies of W 4f at 32.9, 34.9, and 38.3 eV in NiO@Ni/WS_2/CC are lower than those in WS_2/CC (33.0, 35.1, and 38.6 eV), highlighting the interaction between NiO@Ni and WS_2.

Then, we explore the chemical and structural information on NiO@Ni/WS_2/CC insightfully by X-ray absorption near-edge structure (XANES) and extended X-ray absorption fine structure (EXAFS) spectroscopy. The XANES spectrum of Ni K-edge for NiO@Ni/WS_2/CC (Figure 3A) shows a strong blue line signal at 8350 eV, which belongs to NiO. The signal at 8335 eV represents metal Ni which corresponds to the spectrum of Ni foil.[38] Figure 3B shows the Fourier transforms (FTs) of the EXAFS oscillations obtained at the Ni K-edges; the peak at 1.8 Å corresponds to Ni−O interactions followed by two specific Ni−Ni interactions between 3 and 5 Å.[39] According to FTs of the EXAFS simulation (Figure 3C and Table S1), the coordination numbers (N^a) of Ni/O and Ni/Ni are 1.8 at 2.04 Å and 7.2 at 2.48 Å in NiO@Ni/WS_2/CC, respectively, which is quite different from the 6 N^a of Ni/O at 2.08 Å in NiO and 12 N^a of Ni/Ni at 2.48 Å in Ni foil. It is indicated that the interaction between NiO@Ni and WS_2 changes the spatial structure of Ni.[40] The red line of W L3-edge XANES spectrum for NiO@Ni/WS_2/CC (Figure 3D) shows that W has a distorted WO_6 octahedral symmetry.[41] Compared to WS_2/CC, with analysis by the XPS, the lower W L3 intensity for NiO@Ni/WS_2/CC indicates the decreasing W valence caused by the electron transference from Ni and NiO to W.[42] The FTs of the EXAFS oscillations obtained W L3 are shown in Figure 3E; two curves almost overlap, and the R space has not changed, indicating there is no change on the spatial structure of WS_2 in NiO@Ni/WS_2/CC. Thus, it may be that the WS_2 could act to stabilize the NiO@Ni.[43]

There are four peaks of a (∼2471 eV), b (∼2479 eV), c (∼2482 eV), and d (∼2491 eV) in the XANES spectra of sulfur K-edge (Figure 3F).[44,45] It is known that the peak a is generated by the electron transition between S 1s and unoccupied hybridized orbitals of S 3p and W 4f, peaks b and c correspond to the transition to p-like final states.[46] The height of peak c in NiO@Ni/WS_2/CC is obviously higher than that in WS_2/CC, and this peak can be assigned to S atoms in the +6 oxidation state (6^+) due to the similarity with the sharp peak observed in the S K-edge spectrum of $ZnSO_4{\cdot}7H_2O$.[47] As mentioned above, the S−O bond should be attributed to the oxidation of S.

The electrochemical HER performances of NiO@Ni/WS_2/CC, WS_2/CC, NiO@Ni/CC and commercial Pt/C loaded on CC (20 wt % Pt/XC-72, Pt/C/CC) are evaluated at a scan rate of 5 mV s^{-1} in 1.0 M KOH (Figure 4A). Since the intrinsic behavior of electrocatalysts cannot be fully reflected in the measured reaction currents, iR-correction is performed for all the initial data according to the electrical impedance spectroscopy (EIS) for further analysis.[48] As shown in Figure S7, the NiO@Ni/WS_2/CC processes enhanced electrical conductivity when compared to those for pure NiO@Ni/CC and WS_2/CC. As expected, Pt/C/CC demonstrates excellent HER perform-

DOI: 10.1021/acscentsci.7b00502
ACS Cent. Sci. 2018, 4, 112−119

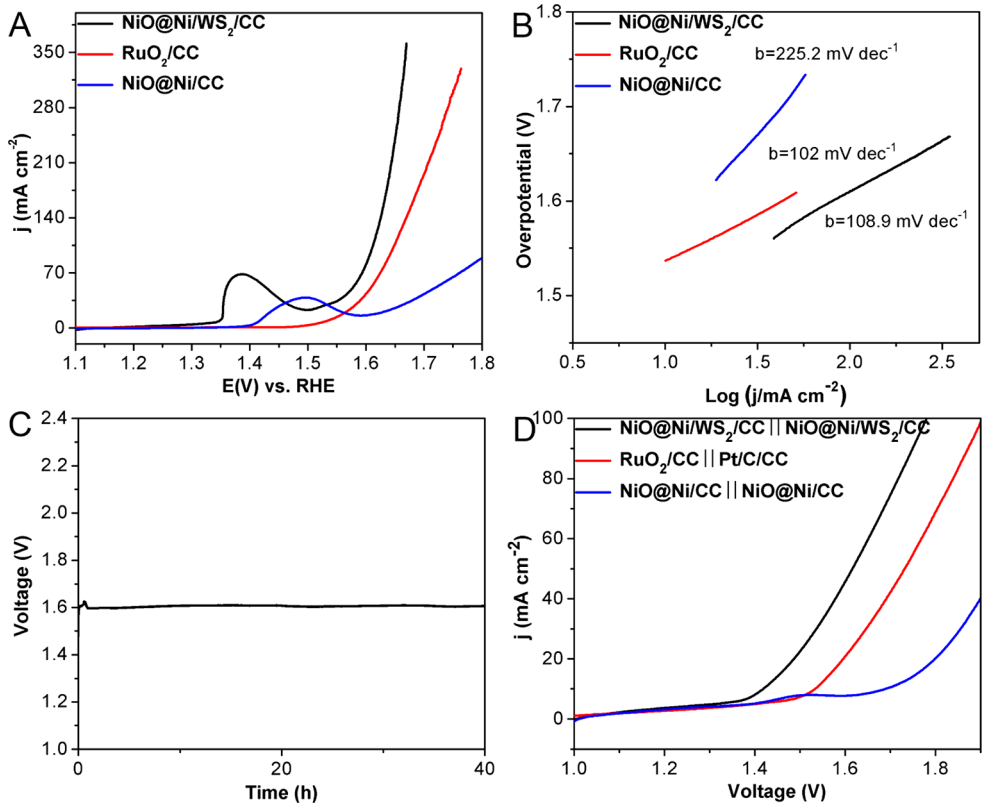

Figure 5. (A) LSV curves for NiO@Ni/WS_2/CC, RuO_2/CC, and NiO@Ni/CC with a scan rate of 5 mV s^{-1} for OER. (B) The corresponding Tafel plots of NiO@Ni/WS_2/CC, RuO_2/CC, and NiO@Ni/CC. (C) Chronopotentiometric curve of NiO@Ni/WS_2/CC with constant current density of 50 mA cm^{-2}. (D) LSV curves of water electrolysis for NiO@Ni/WS_2/CC||NiO@Ni/WS_2/CC, RuO_2/CC||Pt/C/CC, and NiO@Ni/CC||NiO@Ni/CC with a scan rate of 2 mV s^{-1}.

ance with negligible onset overpotential, and only an overpotential of 36 mV is needed to obtain the current density of 10 mA cm^{-2}. The NiO@Ni/WS_2/CC achieves current densities of 10, 20, and 100 mA cm^{-2} at overpotentials of 40, 61, and 117 mV, respectively, which displays better higher activities than those reported non-Pt electrocatalysts at present (Table S2). Furthermore, the performance is very close to that of Pt/C/CC and even exceeds it at large current density (Figure S8). In sharp contrast, the polarization curves of WS_2/CC and NiO@Ni/CC show inferior HER performance with high onset potentials (183 and 167 mV), and overpotentials of 237 and 170 mV are needed to attain the current density of 20 mA cm^{-2}, respectively. To verify the effect of different degrees of oxidation on the synergy, we tested the linear sweep voltammetry (LSV) curves of the samples prepared at different oxidation times (Figure S9); besides, NiO/WS_2/CC is prepared at 200 °C for 120 min to ensure the full oxidation of the sample, and we can see clearly that the HER performance of NiO@Ni/WS_2/CC heated for 30 min is much better than any others, indicating the ratio of NiO and Ni has a significant impact on the electrocatalytic performance. From the corresponding Tafel plots (Figure 4B), Pt/C/CC shows a Tafel slope of 43 mV dec^{-1}. Notably, the Tafel slope of WS_2/CC and NiO@Ni/CC are 234.9 and 136.4 mV dec^{-1}, while the Tafel slope of NiO@Ni/WS_2/CC is as small as 83.1 mV dec^{-1}, indicating a significant enhancement in electrochemical performance. The stability of the NiO@Ni/WS_2/CC is conducted by cyclic voltammogram (CV) measurements. The negligible decay is observed after 1000 cycling tests, suggesting good stability (Figure 4C). In addition, the potential required to deliver 10 mA cm^{-2} is shifted from −0.035 to −0.046 V after 40 h electrolysis according to the long-term electrochemical stability (Figure 4D), highlighting the great long-term stability of NiO@Ni/WS_2/CC. After the cycling test, the morphology of the nanosheet array is well-maintained (Figure S10). Furthermore, the surface composition of the electrode that underwent stability test is further analyzed by XPS (Figure S11), and the characteristic peaks of W 4f and S 2s for NiO@Ni/WS_2/CC are well-preserved. Because of the surface oxides thicken in strongly alkaline conditions, the characteristic peak at 852.7 eV in Ni 2p region for metallic Ni disappeared after 1000 cycles. However, the detailed analysis by XANES and EXAFS demonstrates that the metallic Ni (8335 eV) is still present after 10 h HER testing, and another peak at 8354 eV can be attributed to some kind of Ni oxide (Figure S12).[39,49]

It is reported that the increasing surface area of catalyst may improve electrochemical activity.[50] The nanosheet array of WS_2 provides a 3D scaffold to support NiO and Ni catalysts and further promote the exposure of active sites. To estimate the electrochemically active surface areas (EASA) of NiO@Ni/WS_2/CC, WS_2/CC, and NiO@Ni/CC, the electrochemical double-layer capacitance (C_{dl}) is measured through collected CVs (Figure S13). The values of C_{dl} for NiO@Ni/WS_2/CC, WS_2/CC, and NiO@Ni/CC are 73, 34, and 10 mF cm^{-2}, respectively, indicating that NiO@Ni/WS_2/CC possesses a large EASA and higher surface roughness, which is favorable for the superior electrochemical activity.

We then investigated the OER activity of NiO@Ni/WS_2/CC, commercial RuO_2 deposited on CC (RuO_2/CC) and NiO@Ni/CC in 1.0 M KOH. RuO_2/CC needs 380 mV to

DOI: 10.1021/acscentsci.7b00502
ACS Cent. Sci. 2018, 4, 112−119

achieve current density of 50 mA cm^{-2} (Figure 5A); however, the NiO@Ni/WS_2/CC has an even better performance with an overpotential of 347 mV to reach 50 mA cm^{-2}, which is superior to most reported OER catalysts in alkaline media (Table S3), and NiO@Ni/CC exhibits inferior OER activity. The oxidation peak at 1.4 V can be ascribed to the redox reaction of Ni and NiO.[51] The corresponding Tafel slope of NiO@Ni/WS_2/CC, RuO_2/CC, and NiO@Ni/CC are 108.9, 102, and 225.2 mV dec^{-1} (Figure 5B), respectively, indicating favorable reaction kinetics for NiO@Ni/WS_2/CC. The NiO@Ni/WS_2/CC electrode also displays long-term electrochemical durability (Figure 5C); it can maintain 50 mA cm^{-2} for no less than 40 h. SEM, XPS, XANES, and EXAFS were used to analyze the morphology and element changes after OER testing. As can be seen from the results, the morphology of NiO@Ni/WS_2/CC is well preserved (Figure S14), and the characteristic peak at 852.7 eV in the Ni 2p region also disappeared due to the surface oxides thickening in strongly alkaline condition (Figure S15). The peaks at 8351 and 8365 eV in XANES spectrum of NiO@Ni/WS_2/CC under constant current OER test for 10 h indicate the formation of β-$Ni(OH)_2$.[39,43] The peaks at 1.6 and 2.7 Å are attributed to the Ni−O and Ni−Ni interactions, respectively (Figure S16).

In order to further approach the practical application, we fabricate an electrolyzer which using NiO@Ni/WS_2/CC as both anode and cathode (NiO@Ni/WS_2/CC‖NiO@Ni/WS_2/CC). As shown in Figure 5D, RuO_2/CC‖Pt/C/CC needs 1.53 V to attain 10 mA cm^{-2}, and NiO@Ni/CC‖NiO@Ni/CC displays inferior performance among them. Surprisingly, NiO@Ni/WS_2/CC‖NiO@Ni/WS_2/CC exhibits high performance that can achieve 10 mA cm^{-2} at a cell voltage of 1.42 V, which is the best performance of two-electrode setup at present as far as we know (Table S4). Notably, this two-electrode setup can maintain 10 mA cm^{-2} more than 25 h (Figure S17), indicating the outstanding electrochemical stability during the overall water splitting.

As described above, the NiO@Ni/WS_2/CC is a near-perfect electrocatalyst for water splitting, and the HER process could be described by Volmer−Tafel and Volmer−Heyrovsky pathways in alkaline media.[52,53] The adsorption of H_2O molecules occurs in two pathways, while the H_2O is electrochemically reduced to adsorbed OH^- and H atom (H_{ads}); eventually, the OH^- was desorbed to refresh the surface and H_{ads} is transformed into H_2.[25] Previous reports indicate metal Ni has a suitable binding energy for H atom and NiO can be hydroxylated to dissociation H_2O.[43] In detail, the OH^- can preferentially attach to the NiO sites at the interface due to the localized positively charged Ni^{2+} and more unfilled d-orbitals in Ni^{2+} than that in Ni metal; meanwhile, the nearby Ni sites will promote H-adsorption and thus promote the Volmer method, imparting synergistic catalytic activity to NiO@Ni, and Ni should promote HER, while NiO should favor OER.[39] CC and metal Ni have very good electrical conductivity, which are very beneficial to the electrocatalytic reaction of the electrode. On the other hand, several recent reports have speculated that the unsaturated sulfur atoms could be related to the HER activity; besides, the modified WS_2 could provide a larger contact area for the HER reaction.[54] More importantly, it can stabilize the NiO@Ni and then steady the whole structure of NiO@Ni/WS_2/CC, so the synergies between various composites make it a highly active bifunctional electrocatalyst.

CONCLUSIONS

We innovatively synthesized a WS_2/CC nanosheet array and then decorated NiO@Ni on the surface to obtain NiO@Ni/WS_2/CC. This new composite not only inherits the advantages of each components, but also makes up for the shortcomings of NiO@Ni and WS_2; both HER and OER performance and durability are significantly improvement compared with the pure NiO@Ni/CC and WS_2/CC. As an HER catalyst, its performance is very close to that of Pt/C and superior to the reported non-noble metal electrocatalysts at present. The OER performance is also better than that of commercial RuO_2, thereby making it possible to construct a stable two-electrode alkaline water electrolysis cell with a 10 mA cm^{-2} at a cell voltage of 1.42 V. The high activity of NiO@Ni/WS_2/CC is attributed to the unique nanosheet array structure and electrocatalytic synergetic effects generated by contacting regions between NiO, Ni, and WS_2. This work may open up a new way to prepare highly active bifunctional catalysts to replace noble metal-based catalysts for water splitting devices.

ASSOCIATED CONTENT

Supporting Information

The Supporting Information is available free of charge on the ACS Publications website at DOI: 10.1021/acscentsci.7b00502.

Experimental details, characterizations, and electrochemical properties study (PDF)

AUTHOR INFORMATION

Corresponding Authors

*E-mail for Z.X.: xingzc@ciac.ac.cn.
*E-mail for X.Y.: xryang@ciac.ac.cn.

ORCID

Xiurong Yang: 0000-0003-0021-5135

Notes

The authors declare no competing financial interest.

ACKNOWLEDGMENTS

This work was supported by the National Natural Science Foundation of China (Nos. 21435005, 21627808, and 21603215) and Key Research Program of Frontier Sciences, Chinese Academy of Sciences (No. QYZDY-SSW-SLH019)

REFERENCES

(1) Cobo, S.; Heidkamp, J.; Jacques, P.-A.; Fize, J.; Fourmond, V.; Guetaz, L.; Jousselme, B.; Ivanova, V.; Dau, H.; Palacin, S.; Fontecave, M.; Artero, V. A Janus cobalt-based catalytic material for electro-splitting of water. *Nat. Mater.* **2012**, *11*, 802−807.

(2) Dresselhaus, M. S.; Thomas, I. L. Alternative energy technologies. *Nature* **2001**, *414*, 332−337.

(3) Nocera, D. G. The artificial leaf. *Acc. Chem. Res.* **2012**, *45*, 767−776.

(4) Gong, M.; Zhou, W.; Kenney, M. J.; Kapusta, R.; Cowley, S.; Wu, Y.; Lu, B.; Lin, M.-C.; Wang, D.-Y.; Yang, J.; Hwang, B.-J.; Dai, H. Blending Cr_2O_3 into a NiO−Ni electrocatalyst for sustained water splitting. *Angew. Chem.* **2015**, *127*, 12157−12161.

(5) Du, S.; Ren, Z.; Zhang, J.; Wu, J.; Xi, W.; Zhu, J.; Fu, H. Co_3O_4 nanocrystal ink printed on carbon fiber paper as a large-area electrode for electrochemical water splitting. *Chem. Commun.* **2015**, *51*, 8066−8069.

(6) Jiao, F.; Frei, H. Nanostructured cobalt oxide clusters in mesoporous silica as efficient oxygen-evolving catalysts. *Angew. Chem.* **2009**, *121*, 1873−1876.

DOI: 10.1021/acscentsci.7b00502
ACS Cent. Sci. 2018, 4, 112−119

(7) Robinson, D. M.; Go, Y. B.; Mui, M.; Gardner, G.; Zhang, Z.; Mastrogiovanni, D.; Garfunkel, E.; Li, J.; Greenblatt, M.; Dismukes, G. C. Photochemical water oxidation by crystalline polymorphs of manganese oxides: structural requirements for catalysis. *J. Am. Chem. Soc.* **2013**, *135*, 3494−3501.
(8) Seitz, L. C.; Chen, Z.; Forman, A. J.; Pinaud, B. A.; Benck, J. D.; Jaramillo, T. F. Modeling practical performance limits of photoelectrochemical water splitting based on the current state of materials research. *ChemSusChem* **2014**, *7*, 1372−1385.
(9) Jiao, Y.; Zheng, Y.; Jaroniec, M.; Qiao, S. Z. Design of electrocatalysts for oxygen- and hydrogen-involving energy conversion reactions. *Chem. Soc. Rev.* **2015**, *44*, 2060−2086.
(10) Chen, S.; Kang, Z.; Zhang, X.; Xie, J.; Wang, H.; Shao, W.; Zheng, X.; Yan, W.; Pan, B.; Xie, Y. Highly active Fe sites in ultrathin pyrrhotite Fe_7S_8 nanosheets realizing efficient electrocatalytic oxygen evolution. *ACS Cent. Sci.* **2017**, *3*, 1221−1227.
(11) Voiry, D.; Salehi, M.; Silva, R.; Fujita, T.; Chen, M.; Asefa, T.; Shenoy, V. B.; Eda, G.; Chhowalla, M. Conducting MoS_2 nanosheets as catalysts for hydrogen evolution reaction. *Nano Lett.* **2013**, *13*, 6222−6227.
(12) Li, S.; Wang, Y.; Peng, S.; Zhang, L.; Al-Enizi, A. M.; Zhang, H.; Sun, X.; Zheng, G. Co−Ni-based nanotubes/nanosheets as efficient water splitting electrocatalysts. *Adv. Energy Mater.* **2016**, *6*, 1501661.
(13) Jin, Y.; Wang, H.; Li, J.; Yue, X.; Han, Y.; Shen, P. K.; Cui, Y. Porous MoO_2 nanosheets as non-noble bifunctional electrocatalysts for overall water splitting. *Adv. Mater.* **2016**, *28*, 3785−3790.
(14) Wang, H.; Lee, H.-W.; Deng, Y.; Lu, Z.; Hsu, P.-C.; Liu, Y.; Lin, D.; Cui, Y. Bifunctional non-noble metal oxide nanoparticle electrocatalysts through lithium-induced conversion for overall water splitting. *Nat. Commun.* **2015**, *6*, 7261.
(15) Tang, C.; Cheng, N.; Pu, Z.; Xing, W.; Sun, X. NiSe nanowire film supported on nickel foam: an efficient and stable 3D bifunctional electrode for full water splitting. *Angew. Chem.* **2015**, *127*, 9483−9487.
(16) Sneed, B. T.; Young, A. P.; Jalalpoor, D.; Golden, M. C.; Mao, S.; Jiang, Y.; Wang, Y.; Tsung, C.-K. Shaped Pd−Ni−Pt core-sandwich-shell nanoparticles: influence of Ni sandwich layers on catalytic electrooxidations. *ACS Nano* **2014**, *8*, 7239−7250.
(17) Chen, W.; Wang, H.; Li, Y.; Liu, Y.; Sun, J.; Lee, S.; Lee, J.-S.; Cui, Y. In situ electrochemical oxidation tuning of transition metal disulfides to oxides for enhanced water oxidation. *ACS Cent. Sci.* **2015**, *1*, 244−251.
(18) Cui, Z.; Ge, Y.; Chu, H.; Baines, R.; Dong, P.; Tang, J.; Yang, Y.; Ajayan, P. M.; Ye, M.; Shen, J. Controlled synthesis of Mo-doped Ni_3S_2 nano-rods: an efficient and stable electro-catalyst for water splitting. *J. Mater. Chem. A* **2017**, *5*, 1595−1602.
(19) Yan, Y.; Xia, B.; Li, N.; Xu, Z.; Fisher, A.; Wang, X. Vertically oriented MoS_2 and WS_2 nanosheets directly grown on carbon cloth as efficient and stable 3-dimensional hydrogen-evolving cathodes. *J. Mater. Chem. A* **2015**, *3*, 131−135.
(20) Yang, J.; Shin, H. S. Recent advances in layered transition metal dichalcogenides for hydrogen evolution reaction. *J. Mater. Chem. A* **2014**, *2*, 5979−5985.
(21) Bonde, J.; Moses, P. G.; Jaramillo, T. F.; Norskov, J. K.; Chorkendorff, I. Hydrogen evolution on nano-particulate transition metal sulfides. *Faraday Discuss.* **2009**, *140*, 219−231.
(22) Lukowski, M. A.; Daniel, A. S.; English, C. R.; Meng, F.; Forticaux, A.; Hamers, R. J.; Jin, S. Highly active hydrogen evolution catalysis from metallic WS_2 nanosheets. *Energy Environ. Sci.* **2014**, *7*, 2608−2613.
(23) Subbaraman, R.; Tripkovic, D.; Chang, K.-C.; Strmcnik, D.; Paulikas, A. P.; Hirunsit, P.; Chan, M.; Greeley, J.; Stamenkovic, V.; Markovic, N. M. Trends in activity for the water electrolyser reactions on 3d M(Ni,Co,Fe,Mn) hydr(oxy)oxide catalysts. *Nat. Mater.* **2012**, *11*, 550−557.
(24) Xu, Y.-F.; Gao, M.-R.; Zheng, Y.-R.; Jiang, J.; Yu, S.-H. Nickel/nickel (II) oxide nanoparticles anchored onto cobalt (IV) diselenide nanobelts for the electrochemical production of hydrogen. *Angew. Chem., Int. Ed.* **2013**, *52*, 8546−8550.
(25) Gong, M.; Zhou, W.; Tsai, M.-C.; Zhou, J.; Guan, M.; Lin, M.-C.; Zhang, B.; Hu, Y.; Wang, D.-Y.; Yang, J.; Pennycook, S. J.; Hwang, B.-J.; Dai, H. Nanoscale nickel oxide/nickel heterostructures for active hydrogen evolution electrocatalysis. *Nat. Commun.* **2014**, *5*, 4695.
(26) Smith, R. D. L.; Prévot, M. S.; Fagan, R. D.; Zhang, Z.; Sedach, P. A.; Siu, M. K. J.; Trudel, S.; Berlinguette, C. P. Photochemical route for accessing amorphous metal oxide materials for water oxidation catalysis. *Science* **2013**, *340*, 60−63.
(27) Gao, L.; Wang, X.; Xie, Z.; Song, W.; Wang, L.; Wu, X.; Qu, F.; Chen, D.; Shen, G. High-performance energy-storage devices based on WO_3 nanowire arrays/carbon cloth integrated electrodes. *J. Mater. Chem. A* **2013**, *1*, 7167−7173.
(28) Sun, C.; Zhang, J.; Ma, J.; Liu, P.; Gao, D.; Tao, K.; Xue, D. N-doped WS_2 nanosheets: a high-performance electrocatalyst for the hydrogen evolution reaction. *J. Mater. Chem. A* **2016**, *4*, 11234−11238.
(29) Xu, P.; Han, X.; Wang, C.; Zhou, D.; Lv, Z.; Wen, A.; Wang, X.; Zhang, B. Synthesis of electromagnetic functionalized nickel/polypyrrole core/shell composites. *J. Phys. Chem. B* **2008**, *112*, 10443−10448.
(30) Del Corro, E.; Botello-Méndez, A.; Gillet, Y.; Elias, A. L.; Terrones, H.; Feng, S.; Fantini, C.; Rhodes, D.; Pradhan, N.; Balicas, L.; Gonze, X.; Charlier, J. C.; Terrones, M.; Pimenta, M. A. Atypical exciton−phonon interactions in WS_2 and WSe_2 monolayers revealed by resonance raman spectroscopy. *Nano Lett.* **2016**, *16*, 2363−2368.
(31) Mironova-Ulmane, N.; Kuzmin, A.; Steins, I.; Grabis, J.; Sildos, I.; Pärs, M. Raman scattering in nanosized NiO. *J. Phys.: Conf. Ser.* **2007**, *93*, 012039.
(32) Tran, P. D.; Chiam, S. Y.; Boix, P. P.; Ren, Y.; Pramana, S. S.; Fize, J.; Artero, V.; Barber, J. Novel cobalt/nickel-tungsten-sulfide catalysts for electrocatalytic hydrogen generation from water. *Energy Environ. Sci.* **2013**, *6*, 2452−2459.
(33) Liang, X.; Liu, B.; Zhang, J.; Lu, S.; Zhuang, Z. Ternary Pd-Ni-P hybrid electrocatalysts derived from Pd-Ni core-shell nanoparticles with enhanced formic acid oxidation activity. *Chem. Commun.* **2016**, *52*, 11143−11146.
(34) Yu, M.; Wang, W.; Li, C.; Zhai, T.; Lu, X.; Tong, Y. Scalable self-growth of Ni@NiO core-shell electrode with ultrahigh capacitance and super-long cyclic stability for supercapacitors. *NPG Asia Mater.* **2014**, *6*, e129.
(35) Zhang, C.; Qian, L.; Zhang, K.; Yuan, S.; Xiao, J.; Wang, S. Hierarchical porous Ni/NiO core-shells with superior conductivity for electrochemical pseudo-capacitors and glucose sensors. *J. Mater. Chem. A* **2015**, *3*, 10519−10525.
(36) Zhao, X.; Ma, X.; Sun, J.; Li, D.; Yang, X. Enhanced catalytic activities of surfactant-assisted exfoliated WS_2 nanodots for hydrogen evolution. *ACS Nano* **2016**, *10*, 2159−2166.
(37) Zhu, H.; Zhang, J.; Yanzhang, R.; Du, M.; Wang, Q.; Gao, G.; Wu, J.; Wu, G.; Zhang, M.; Liu, B.; Yao, J.; Zhang, X. When cubic cobalt sulfide meets layered molybdenum disulfide: A core−shell system toward synergetic electrocatalytic water splitting. *Adv. Mater.* **2015**, *27*, 4752−4759.
(38) Tsai, C.-W.; Chen, H. M.; Liu, R.-S.; Asakura, K.; Chan, T.-S. Ni@NiO core−shell structure-modified nitrogen-doped $InTaO_4$ for solar-driven highly efficient CO_2 reduction to methanol. *J. Phys. Chem. C* **2011**, *115*, 10180−10186.
(39) Liu, X.; Liu, W.; Ko, M.; Park, M.; Kim, M. G.; Oh, P.; Chae, S.; Park, S.; Casimir, A.; Wu, G.; Cho, J. Metal (Ni, Co)-metal oxides/graphene nanocomposites as multifunctional electrocatalysts. *Adv. Funct. Mater.* **2015**, *25*, 5799−5808.
(40) Chen, W.-F.; Sasaki, K.; Ma, C.; Frenkel, A. I.; Marinkovic, N.; Muckerman, J. T.; Zhu, Y.; Adzic, R. R. Hydrogen-evolution catalysts based on non-noble metal nickel−molybdenum nitride nanosheets. *Angew. Chem., Int. Ed.* **2012**, *51*, 6131−6135.
(41) Balerna, A.; Bernieri, E.; Burattini, E.; Kuzmin, A.; Lusis, A.; Purans, J.; Cikmach, P. XANES studies of MeO_{3-x} (Me = W, Re, Ir) crystalline and amorphous oxides. *Nucl. Instrum. Methods Phys. Res., Sect. A* **1991**, *308*, 240−242.
(42) Zhang, B.; Zheng, X.; Voznyy, O.; Comin, R.; Bajdich, M.; García-Melchor, M.; Han, L.; Xu, J.; Liu, M.; Zheng, L.; García de

DOI: 10.1021/acscentsci.7b00502
ACS Cent. Sci. 2018, 4, 112−119

Arquer, F. P.; Dinh, C. T.; Fan, F.; Yuan, M.; Yassitepe, E.; Chen, N.; Regier, T.; Liu, P.; Li, Y.; De Luna, P.; Janmohamed, A.; Xin, H. L.; Yang, H.; Vojvodic, A.; Sargent, E. H. Homogeneously dispersed multimetal oxygen-evolving catalysts. *Science* **2016**, *352*, 333−337.
(43) Bates, M. K.; Jia, Q.; Ramaswamy, N.; Allen, R. J.; Mukerjee, S. Composite Ni/NiO-Cr_2O_3 catalyst for alkaline hydrogen evolution reaction. *J. Phys. Chem. C* **2015**, *119*, 5467−5477.
(44) Cai, L.; He, J.; Liu, Q.; Yao, T.; Chen, L.; Yan, W.; Hu, F.; Jiang, Y.; Zhao, Y.; Hu, T.; Sun, Z.; Wei, S. Vacancy-Induced ferromagnetism of MoS_2 nanosheets. *J. Am. Chem. Soc.* **2015**, *137*, 2622−2627.
(45) Guay, D.; Divigalpitiya, W. M. R.; Belanger, D.; Feng, X. H. Chemical bonding in restacked single-layer MoS_2 by X-ray absorption spectroscopy. *Chem. Mater.* **1994**, *6*, 614−619.
(46) Li, D.; Bancroft, G. M.; Kasrai, M.; Fleet, M. E.; Feng, X. H.; Tan, K. H. Polarized X-ray absorption spectra and electronic structure of molybdenite (2H-MoS_2). *Phys. Chem. Miner.* **1995**, *22*, 123−128.
(47) Zubavichus, Y. V.; Slovokhotov, Y. L.; Schilling, P. J.; Tittsworth, R. C.; Golub, A. S.; Protzenko, G. A.; Novikov, Y. N. X-ray absorption fine structure study of the atomic and electronic structure of molybdenum disulfide intercalation compounds with transition metals. *Inorg. Chim. Acta* **1998**, *280*, 211−218.
(48) Popczun, E. J.; McKone, J. R.; Read, C. G.; Biacchi, A. J.; Wiltrout, A. M.; Lewis, N. S.; Schaak, R. E. Nanostructured nickel phosphide as an electrocatalyst for the hydrogen evolution reaction. *J. Am. Chem. Soc.* **2013**, *135*, 9267−9270.
(49) Mansour, A. N.; Melendres, C. A.; Pankuch, M.; Brizzolara, R. A. X-ray absorption fine structure spectra and the oxidation state of nickel in some of its oxycompounds. *J. Electrochem. Soc.* **1994**, *141*, L69−L71.
(50) Xie, J.; Li, S.; Zhang, X.; Zhang, J.; Wang, R.; Zhang, H.; Pan, B.; Xie, Y. Atomically-thin molybdenum nitride nanosheets with exposed active surface sites for efficient hydrogen evolution. *Chem. Sci.* **2014**, *5*, 4615−4620.
(51) Louie, M. W.; Bell, A. T. An investigation of thin-film Ni−Fe Oxide catalysts for the electrochemical evolution of oxygen. *J. Am. Chem. Soc.* **2013**, *135*, 12329−12337.
(52) Vilekar, S. A.; Fishtik, I.; Datta, R. Kinetics of the hydrogen electrode reaction. *J. Electrochem. Soc.* **2010**, *157*, B1040−B1050.
(53) Skúlason, E.; Tripkovic, V.; Björketun, M. E.; Gudmundsdóttir, S.; Karlberg, G.; Rossmeisl, J.; Bligaard, T.; Jónsson, H.; Nørskov, J. K. Modeling the electrochemical hydrogen oxidation and evolution reactions on the basis of density functional theory calculations. *J. Phys. Chem. C* **2010**, *114*, 18182−18197.
(54) Wang, T.; Liu, L.; Zhu, Z.; Papakonstantinou, P.; Hu, J.; Liu, H.; Li, M. Enhanced electrocatalytic activity for hydrogen evolution reaction from self-assembled monodispersed molybdenum sulfide nanoparticles on an Au electrode. *Energy Environ. Sci.* **2013**, *6*, 625−633.

DOI: 10.1021/acscentsci.7b00502
ACS Cent. Sci. 2018, 4, 112−119